Quantifying Post-Wildfire Hillslope Erosion with lidar

Francis Rengers
U.S. Geological Survey
Landslide Hazards Program
Golden, Colorado, USA
frengers@usgs.gov

Luke McGuire
University of Arizona
Department of Geosciences
Tucson, Arizona, USA

Abstract—**Following a wildfire, flooding and debris- flow hazards are common and pose a threat to human life and infrastructure in steep burned terrain. Wildfire enhances both water runoff and soil erosion, which ultimately shape the debris flow potential. The erosional processes that route excess sediment from hillslopes to debris-flow channels in recently burned areas, however, are poorly constrained. In this study we examined erosional processes through repeat terrestrial lidar surveys in a steep mountainous watershed that experienced a high-severity burn in the 2016 San Gabriel complex fire. Three lidar surveys were conducted during a wet winter (2016-2017) on a hillslope plot. We used geomorphometric techniques to better contextualize erosion observations in areas with rills and between rills (interrill areas). A challenge was effectively differentiating DEM pixels that were in the constantly evolving rill network as well as those outside the rill network. By applying a series of DEM filtering processes we found that it was possible to efficiently identify the small-scale rill networks. Our results challenge prior observations that sediment erosion on burned hillslopes is dominated by rill erosion, suggesting that prior estimates made without access to high resolution topography likely underestimated the role of interrill erosion.**

I. Introduction

Debris flows are a major threat to infrastructure and human life in burned landscapes [1], and one of the key questions for understanding debris flows is: where does the debris flow sediment originate? Prior studies have suggested that debris flows can initiate in rills and then accumulate more material as they move downstream [2, 3]. This would suggest that at a hillslope-scale much of the sediment erosion would likely originate in rills. Moreover, many prior researchers have suggested that rill erosion is the dominant hillslope erosion mechanism in burn areas in the western United States [4, 5, 6, 7].

Therefore, constructing a mass-balance at a hillslope-scale to show the proportion of sediment eroded in rills versus the rest of the hillslope could help to inform our understanding of the sedimentation risks in a burn area. Moreover, by identifying where the most erosion happens on a hillslope we can also define different erosional process domains and improve predictive models. For example, it has been shown that the majority of erosion in interrill areas is typically due to rainsplash, rather than runoff [8].

A key challenge, however, is that rill widths and depths are typically centimeters to decimeters, making it difficult to perform a controlled mass-balance of sediment erosion at the hillslope scale. Herein we use high-precision surface elevation measurements to quantify rill and interrill erosional changes in a burn area using three digital elevation models (DEMs) with 2.5 cm pixel-resolution derived from ground-based lidar. We seek to partition erosion by using geomorphometric approaches to define rill and interrill areas. In particular we focused on extracting the active rill network from each DEM by using a combination of DEM processing methods. With this network of erosional channels we can better understand how erosion occurs within and outside of the rill network in a burned landscape.

II. Methods

We conducted three repeat surveys on a burned hillslope using a Leica ScanStation C10 terrestrial laser scanner (TLS) (Fig. 1), within a four-month period. The first TLS scan was conducted after the wildfire and prior to any rainfall. The second TLS scan was obtained following several rain events. The third TLS scan took place following several more rain events and after the regrowth of vegetation. Vegetation removal from the point cloud was conducted using the CANUPO plug-in (CloudCompare software), and the point cloud was further processed using the vegetation filtering method in LAStools.

With this lidar data we sought to quantify the erosion in rill areas and interrill areas on the hillslope, but a pre-requisite to this analysis was to correctly identify the rill and interrill areas. To do this we used a series of geomorphic criteria to determine rill locations.

A Gaussian filter was applied to the DEM using:

$$GDEM(x,y) = \frac{1}{2\pi\sigma^2} e^{-\frac{x^2+y^2}{2\sigma^2}}$$

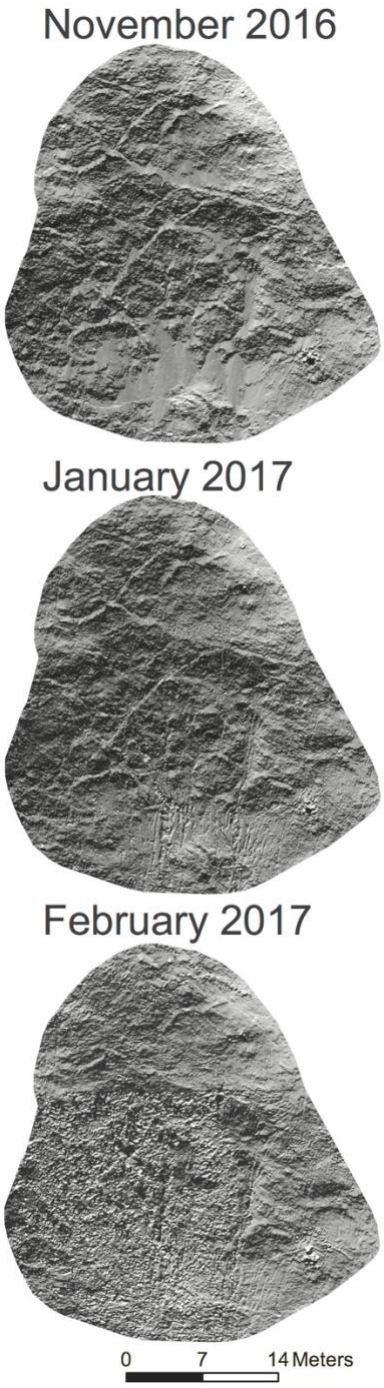

Figure 1. Hillshade plots showing terrestrial lidar results (top) before any runoff and erosion, (center) after the first rainfall, (bottom) after several more rainstorms and with the regrowth of vegetation.

where σ is the standard deviation of elevation, and x and y are spatial coordinates. All areas with depressions were then identified using the difference between the GDEM and the original DEM:

$$GDEM_{diff} = DEM - GDEM$$

Because all rills are depressions, but not all depressions are rills, we next used the D-infinity drainage area to extract areas that were identified as depressions in the $GDEM_{diff}$ and also had a high drainage area. This effectively identified areas in the DEM that were rill pathways; however, we also wanted to know if the rills were new or existed on the landscape prior to the lidar scan. To determine new, or actively eroding, rills versus inactive rills, we calculated a DEM of Difference (DoD) as:

$$DoD = DEM_{i+1} - DEM_i$$

where *i* indicates the lidar survey epoch. If a pixel in a rill incised more than 2 cm between the lidar surveys, it was considered to be active. By using this criterion, we also excluded pixels less than our lidar vertical position uncertainty, which is typically ~6mm for our lidar unit. Consequently, we identified all active areas in the rill pathways and extracted these portions of the DEM to determine the active rills. All areas outside of the rill pixels were assumed to be interrill pixels.

III. Results

The DEM-defined rill-network allowed us to extract landscape metrics and to learn more about the spatial distribution of erosion on the landscape (Table 1). In particular we found that the total erosion on the hillslope plot was much higher in interrill areas than rill areas. Once sediment is eroded from an interrill it can leave the landscape via transport in a rill but since the primary erosion mechanism is not due to rilling, interrill erosion is considered separately. In addition, we saw that the mean rill length and rill erosion decreased over time. Such that the original erosional pulse due to rilling was highest after the first rainstorms and declined with time.

To see how erosion changed across the entire landscape and with respect to different geomorphic process areas, we investigated how erosion was distributed with respect to slope-area curves of the hillslope (Fig. 4). We found that for both DEMs with rill erosion (January and February 2017) the erosion volume was highest at low drainage areas and decreased at higher drainage areas. This indicates that the majority of the sediment volume that was eroded was from interrill areas. By contrast, the mean erosion within a particular drainage area bin tended to increase with drainage area. This shows that rills, which occupy

areas of higher drainage area, erode more sediment per pixel (but less total volume) than the low drainage area interrill areas.

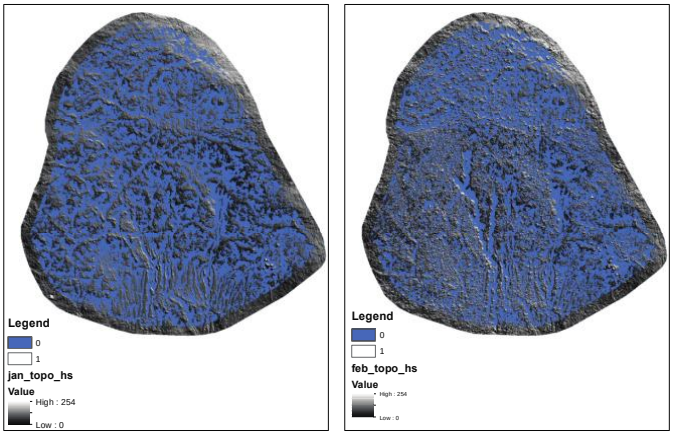

Figure 2. A Gaussian filter was applied to the elevation data derived from the January and February 2017 lidar data. Using python we imported the Gaussian filter package. A standard deviation of 10 was used for the Gaussian filter. The smoothed filtered data was subsequently subtracted from the original elevation data. Depressions were identified as the negative areas, displayed in blue. (Left) January 2017 hillshade with depressions displayed in blue. (Right) February 2017 hillshade with depressions displayed in blue.

IV. Discussion

High resolution terrestrial lidar data are useful for highlighting centimeter-scale changes by DEM differencing. However, understanding elevation change is more useful within the context of generalizable landscape units rather than on a pixel-by-pixel basis. For example, in this study we sought to understand how erosion patterns differed between rill and interrill areas. To contextualize the lidar-derived elevation change in our study landscape, it was first necessary to categorize portions of the lidar DEM into rill and interrill areas.

Our results suggest that while mean pixel erosion is highest in rill areas, the total volume of material eroded from the landscape is primarily derived from low drainage area interrill areas. This observation points toward the erosional processes that may be the most important in driving erosion at the hillslope scale, (i.e. rainsplash detachment of material in low drainage area portions of the landscape [8]). Thus rainsplash, as opposed to hillslope rilling, must be driving overall hillslope erosion.

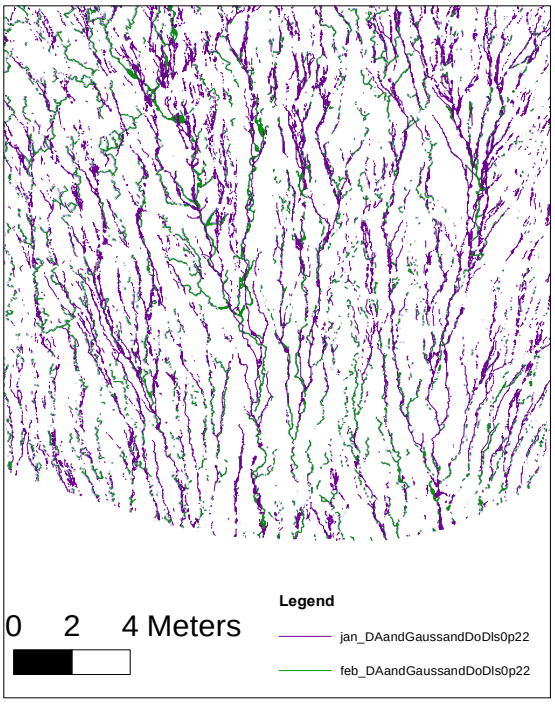

Figure 3. The final extracted rill network is shown for a portion of the study area. The rills from the January 2017 lidar scan are shown in blue and the February 2017 rill network is shown in green.

TABLE I. Lidar-derived metrics that show the spatial distribution of erosion

Rill Erosion Metrics		
Metric	***January 2017***	***February 2017***
Rill Length (m)	2200	960
Total Rill Erosion (m^3)	2.3	1.8
Total Interrill Erosion (m^3)	13	16.4
Mean Rill Erosion (m)	0.05	0.19
Mean Interrill Erosion (m)	0.014	0.018

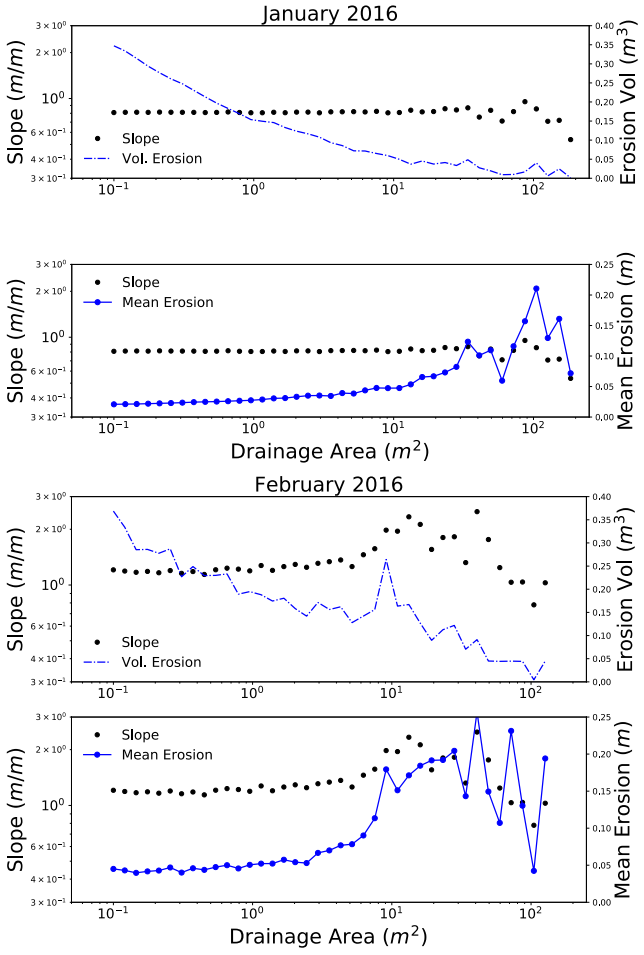

Figure 4. The distribution of the total eroded volume and the mean erosion on the landscape contextualized using a slope-area plot.

V. CONCLUSIONS

This study uses terrestrial lidar to track erosion patterns on a burned hillslope area. Using a Gaussian DEM difference, in conjunction with erosion thresholds from DEM differencing, and drainage area from D-infinity flow routing methods we identified a discontinuous active rill network from the lidar-derived DEMs. Through this DEM analysis it was possible to investigate the relative amount of erosion on different parts of the landscape. Our results show that despite the deep incision from rilling, the majority of erosion occurs in interrill areas. This result is in contrast to prior observational studies in areas without high-precision lidar [4, 5, 6, 7], but it is consistent with hillslope erosion studies that have used terrestrial lidar [9, 10, 11].

ACKNOWLEDGMENT

The use of trade, product or firm names in this paper is for descriptive purposes only and does not constitute endorsement by the US Geological Survey.

REFERENCES

[1] Santi, P. M., Cannon, S., DeGraff, J., 2013. Wildfire and landscape change. In: Shroder, J., James, L.A., Harden, C.P., Clague, J.J. (Eds.), Treatise on Geomorphology. Acad. Pr., San Diego, CA, v. 13, Geomorphology of Human Disturbances, Climate Change, and Natural Hazards, pp. 262-287.

[2] Cannon, S.H., Bigio, E.R., Mine, E., 2001. A process for fire-related debris flow initiation, Cerro Grande fire, New Mexico. Hydrol. Process. 15, 3011–3023.

[3] Schmidt, K.M., Hanshaw, M.N., Howle, J.F., Kean, J.W., Staley, D.M., Stock, J.D., Bawden, G.W., 2011. Hydrologic conditions and terrestrial laser scanning of post-fire debris flows in the San Gabriel Mountains, CA, U.S.A. In: Genevois, R., Hamilton, D.L., Prestininzi, A. (Eds.), Proc. of the 5th Int. Conf. on Debris Flow Hazards Mitigation/Mechanics, Prediction, and Assessment, Padua, Italy, June, 2011. Italian Journal of Engineering Geology and Environment-Book. Casa Editrice Universita La Sapienza, Rome, Italy, pp. 583–593.

[4] Moody, J.A., Martin, D.A., 2001. Initial hydrologic and geomorphic response following a wildfire in the Colorado Front Range. Earth Surf. Process. Landf. 26, 1049–1070.

[5] Moody, J.A., Kinner, D.A., 2006. Spatial structures of stream and hillslope drainage networks following gully erosion after wildfire. Earth Surf. Process. Landf. 31, 319–337.

[6] Robichaud PR, Wagenbrenner JW, Brown RE. 2010. Rill erosion in natural and disturbed forests: 1. Measurements. Wat. Res. Rsrch. 46: W10506. DOI: 10.1029/2009wr008314

[7] Wagenbrenner, J., Robichaud, P., 2013. Post-fire bedload sediment delivery across spatial scales in the interior western United States. Earth Surf. Process. Landf. 39 (7), 865–876.

[8] McGuire, L. A., J. W. Kean, D. M. Staley, F. K. Rengers, and T. A. Wasklewicz, 2016. Constraining the relative importance of raindrop- and flow-driven sediment transport mechanisms in post-wildfire environments and implications for recovery time scales, *J. Geophys. Res. Earth Surf.*, *121*, 2211–2237, doi:10.1002/2016JF003867.

[9] Staley, D., Wasklewicz, T., Kean, J., 2014. Characterizing the primary material sources and dominant erosional processes for post-fire debris-flow initiation in a headwater basin using multi-temporal terrestrial laser scanning data. Geomorph.214, 324–338.

[10] Rengers, F., Tucker, G., Moody, J., Ebel, B., 2016. Illuminating wildfire erosion and deposition patterns with repeat terrestrial lidar. J. Geophys. Res. Earth Surf. 121, 3, 588–608.

[11] DeLong, S. B., Youberg, A. M., DeLong, W. M., & Murphy, B. P., 2018. Post-wildfire landscape change and erosional processes from repeat terrestrial lidar in a steep headwater catchment, Chiricahua Mountains, Arizona, USA. Geomorph., *300*, 13-30.